ADVANCED FUNCTIONAL MATERIALS

www.afm-journal.de

Liquid Metal Supercooling for Low-Temperature Thermoelectric Wearables

*Mohammad H. Malakooti, Navid Kazem, Jiajun Yan, Chengfeng Pan, Eric J. Markvicka, Krzysztof Matyjaszewski, and Carmel Majidi**

Elastomers embedded with droplets of liquid metal (LM) alloy represent an emerging class of soft multifunctional composites that have potentially transformative impact in wearable electronics, biocompatible machines, and soft robotics. However, for these applications it is crucial for LM alloys to remain liquid during the entire service temperature range in order to maintain high mechanical compliance throughout the duration of operation. Here, LM-based functional composites that do not freeze and remain soft and stretchable at extremely low temperatures are introduced. It is shown that the confinement of LM droplets to micro-/nanometer length scales significantly suppresses their freezing temperature (down to −84.1 from −5.9 °C) and melting point (down to −25.6 from +17.8 °C) independent of the choice of matrix material and processing conditions. Such a supercooling effect allows the LM inclusions to preserve their fluidic nature at low temperatures and stretch with the surrounding polymer matrix without introducing significant mechanical resistance. These results indicate that LM composites with highly stabilized droplets can operate over a wide temperature range and open up new possibilities for these emerging materials, which are demonstrated with self-powered wearable thermoelectric devices for bio-sensing and personal health monitoring at low temperatures.

1. Introduction

Liquid metal-embedded elastomers (LMEEs) represent a class of soft multifunctional composites fabricated by dispersing nano-/microscale liquid metal (LM) inclusions within an elastomer matrix, usually polydimethylsiloxane (PDMS).[1–6] In contrast to rigid filler particles, the embedded LM droplets are highly deformable and can stretch with the surrounding elastomer without introducing significant mechanical resistance or inducing internal stress concentrations. Moreover, because they are metallic, the droplets can serve as functional units for tailoring the electric permittivity, thermal conductivity, or electrical conductivity of the composite. The combination of rubbery matrices and liquid-phase inclusions has enabled the development of highly compliant and stretchable composites with exceptional thermal or electrical performance. These properties include high dielectric constant and breakdown,[7–9] enhanced thermal conductivity,[10–13] high electrical conductivity with limited electromechanical coupling,[14–18] extreme toughness,[19–22] and electrically self-healing ability.[23–25] However, despite the extraordinary promise of LMEEs, a potential limitation for their use in real-world applications is the relatively high crystallization temperature of the metal alloys used for the dispersion phase. The limitation on working temperature becomes more pronounced when microfluidic channels with enclosed bulk LM or solder alloys are utilized as flexible electronics.[26–30]

Eutectic gallium indium (EGaIn) alloy is typically used as the LM dispersion within LMEE composites (**Figure 1**a). As with other Ga-based LM alloys, EGaIn (75 wt% Ga 25 wt% In)

Dr. M. H. Malakooti, C. F. Pan
Mechanical Engineering Department
Carnegie Mellon University
Pittsburgh, PA 15213, USA

Dr. N. Kazem
Civil and Environmental Engineering Department
Carnegie Mellon University
Pittsburgh, PA 15213, USA

Dr. J. J. Yan, Prof. K. Matyjaszewski
Chemistry Department
Carnegie Mellon University
Pittsburgh, PA 15213, USA

Prof. E. J. Markvicka
Mechanical and Materials Engineering Department
University of Nebraska
Lincoln, NE 68588, USA

Prof. C. Majidi
Mechanical Engineering Department
Civil and Environmental Engineering Department
Robotics Institute
Carnegie Mellon University
Pittsburgh, PA 15213, USA
E-mail: cmajidi@andrew.cmu.edu

The ORCID identification number(s) for the author(s) of this article can be found under https://doi.org/10.1002/adfm.201906098.

DOI: 10.1002/adfm.201906098

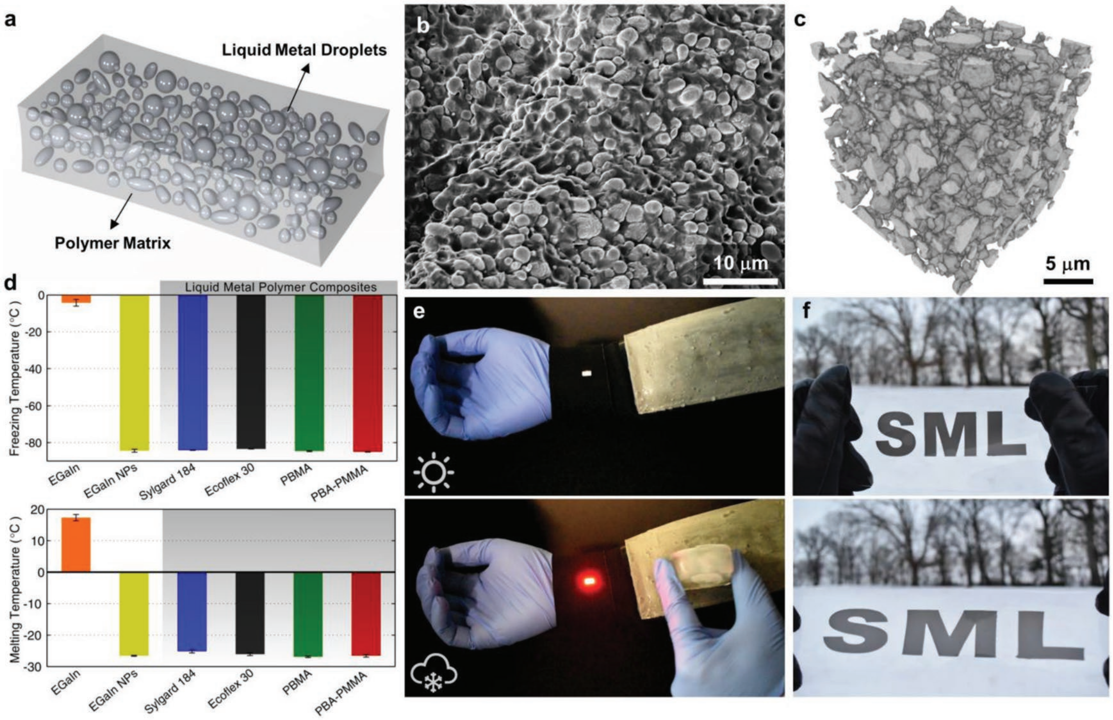

Figure 1. Tailored soft and stretchable multifunctional composites for extreme low temperatures. a) Schematic of LM-embedded elastomer (LMEE). b) A cross-section SEM image of LMEE (50% volume fraction of EGaIn droplets with an average diameter of ≈2 μm embedded in Sylgard 184). c) 3D Nano-CT of the LMEE composite. d) Freezing and melting temperatures (peak value) of bulk EGaIn, EGaIn NDs (≈500 nm diameter), and embedded EGaIn droplets in different polymer matrices (shaded background indicates EGaIn composites). e) A wearable TEG powering a red LED light under an approximately 37 °C temperature gradient simulating extreme cold weather conditions. f) Demonstrating the stretchability of tailored LMEE composites at low temperatures.

has high electrical conductivity (3.4×10^6 S m^{-1}),[1,26] thermal conductivity (26.4 W m^{-1} K^{-1}),[10,31] low viscosity (2.0×10^{-3} Pa s),[32,33] and negligible toxicity.[15,34] However, bulk EGaIn has an onset freezing and melting temperature of -11 ± 6 and 15.5 ± 3 °C, respectively. The difference between these two temperatures is due to the supercooling effect of EGaIn, which has been commonly observed in LMs, particularly with Ga and Ga-based alloys.[30,35] Similarly, Ga-In-Sn ("Galinstan") alloys have phase transition temperatures that are slightly lower (a melting point of −19 °C[30]), but still well above the freezing point or glass transition temperature of most polymer matrix materials. For instance, Sylgard 184, which is a popular silicone elastomer for soft microfluidics, has a glass transition temperature of −130 °C.[36,37] While this temperature mismatch is not an important factor for room-temperature applications, it can potentially be limiting for uses in extreme weather conditions, deep-sea underwater applications, and space technologies. In particular, LM freezing during low temperature applications can result in increased rigidity, high internal stress concentrations, embrittlement, inelasticity, and other sources of mechanical degradation that typically arise with high concentrations of rigid filler particles.[38,39] For instance, in a recent study on dielectric behavior of LMEEs at low temperatures, the importance of the LM and matrix crystallization on the functional and structural response of LMEEs was perceived.[9] Therefore, understanding the influence of temperature on the phase composition and mechanical properties of LMEEs is critical for establishing its applicability in a wide range of engineering applications. Moreover, such a comprehensive study on the thermal stability of LM droplets provides new insights on the potential role of material processing, size effects, supercooling, and dispersion medium on crystallization and melting temperature depression of Ga-based alloys.

Here, we address this challenge with a systematic study that examines the phase composition and mechanical properties of a variety of LM-based material systems at low temperatures. These include comparisons of the freezing and melting points for bulk EGaIn, EGaIn nanodroplets (NDs), and EGaIn-based composites with various LM droplet sizes and polymer compositions. In previous works, low melting temperature metals were shear mixed in an uncured elastomer carrier using a planetary mixer to fabricate LMEEs. The average size of EGaIn droplets in these composites is approximately 50–140 μm[3,23] for Sylgard 184 and 20 μm[19] for Ecoflex 00–30 with a filler volume fraction of 50%. In this work, we present immersion shear mixing as an alternative fabrication process for scalable synthesis of LMEEs with tunable LM droplet size. As shown in Figure 1b,c, an average size of ≈2 μm is achieved for EGaIn droplets in a 50% Sylgard LMEE which is one order of magnitude smaller than what was previously achieved with centrifugal planetary mixing. Figure S1 in the Supporting Information shows the micrographs and diameter histograms of 50% Sylgard LMEE composites prepared by immersion and centrifugal planetary mixing methods. Stabilized EGaIn nano-/microdroplets have significantly lower crystallization temperature (as low as –85 °C) and melting point (down to –26 °C) with significantly enhanced supercooling effect, as illustrated in Figure 1d. This suppression of phase transition temperature is independent of matrix materials and synthesis process as we show this behavior of EGaIn droplets in LM-composites with both thermoset and thermoplastic matrices prepared by different synthesis methods. This phenomenon significantly broadens the range of applications and operational temperature for LM-based electronics and devices. For instance, coupling the high thermal conductivity and depressed freezing-point of LM droplets makes LMEEs suitable for wearable thermoelectric energy harvesters in extreme cold environments (Figure 1e,f and Video S1, Supporting Information). That is, LMEEs can be cooled down to low temperatures and remain soft, stretchable, and still multifunctional when the droplets are sufficiently small and the matrix material is carefully selected (i.e., Sylgard 184 is used vs Ecoflex 00–30) to eliminate freezing of both filler and matrix. Introducing highly stable LM droplets within elastomers and understanding their thermal behavior will provide new opportunities to apply LM-elastomer composites for thermoelectric and low temperature applications.

2. Results and Discussion

2.1. Thermo-Mechanical Behavior

Experiments were primarily performed with Sylgard 184 as the elastomer matrix, which was selected because it remains rubbery at temperatures below –100 °C.[36,37] In contrast, Ecoflex 00–30, another popular silicone for LMEE composites, shows the onset of crystallization at a temperature of –61.5 °C (Figure S2, Supporting Information).[9,40] The thermo-mechanical behavior of the Sylgard-based LMEE composite and unfilled Sylgard at low temperatures were characterized using dynamic mechanical analysis (DMA) and differential scanning calorimetry (DSC). The specimens are subjected to a cooling–heating cycle to investigate any possible phase transition in LM droplets. As shown in **Figure 2**a–c, LMEE and unfilled PDMS specimens show a similar thermo-mechanical behavior without any solidification or melting phase transition in the range of +30 to –80 °C. Addition of LM droplets into PDMS matrix does not alter the storage modulus, loss modulus, or damping ratio (tan δ) and both specimens remain soft and stretchable in this temperature range. Compared to unfilled PDMS, there is a slight increase in the initial value of the storage modulus and loss modulus of LMEE specimens. As the temperature reduces, the difference in storage and loss moduli of LMEE and PDMS decreases and fully disappears at –80 °C. As the temperature increases during the heating step, the difference in elastic modulus is observed to return. This behavior indicates that the presence of LM droplets in fact lessens the relative increase in elastic modulus of PDMS as it is cooled down to lower temperatures.

Negligible hysteresis is observed in an unfilled PDMS sample while the LMEE sample showed small hysteresis between the cooling and heating stages of the temperature cycling. We postulate that a very small portion of LM droplets undergoes freezing or that partial crystallization may be occurring during the cooling

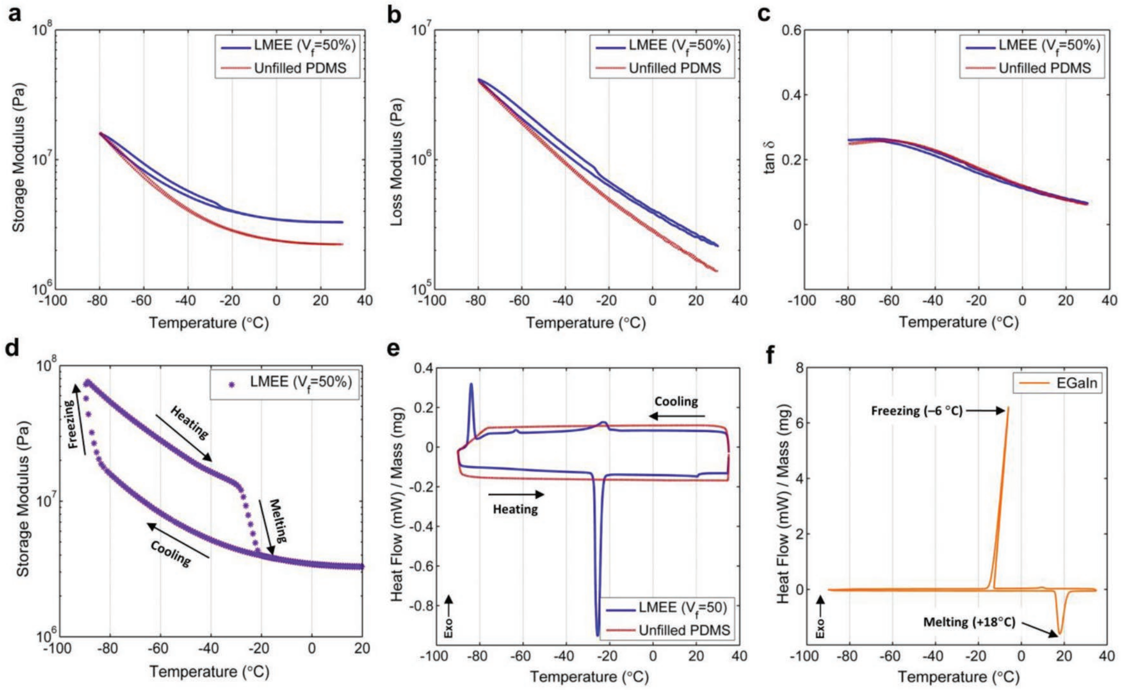

Figure 2. Thermo-mechanical characterization of LMEE composites. a) Storage modulus, b) loss modulus, and c) damping ratio (tan δ) of LMEE (50% volume fraction of EGaIn droplets with an average diameter of ≈2 µm embedded in Sylgard 184) and unfilled PDMS (Sylgard 184) as a function of temperature at 1% strain measured by DMA. d) Storage modulus of the LMEE composite when it is cooled down to –85 °C. e) Normalized DSC heat flux as a function of temperature for the LMEE composite and unfilled PDMS. f) DSC curve for bulk EGaIn showing its freezing and melting points.

step since as the temperature increases the hysteresis behavior disappears at −26 °C, which is the melting point of EGaIn droplets. Regardless of this small phase change, the DMA results indicate that LMEE specimens are able to withstand temperatures down to −80 °C without showing major stiffening or change in energy dissipation capacity. Such results imply that the LMEE composites remain soft and stretchable at extreme cold environments. It is worth noting that if the temperature is brought down to −82 °C or lower, the embedded LM droplets crystallize and the storage modulus of LMEE specimen significantly increases as shown in Figure 2d. As expected, the frozen LM droplets begin melting at −26 °C during the heating step and the original storage modulus of LMEE is fully recovered at −20 °C.

The thermo-mechanical behavior of LMEE at low temperatures is consistent with measurements performed through DSC analysis. As shown in Figure 2e, LMEE specimens with an average diameter of 2 µm show a peak freezing temperature of −84.1 °C (onset = −82.4 °C) and a peak melting temperature of −25.6 °C (onset = −27.7 °C) while the unfilled PDMS does not have any peaks corresponding to either freezing or melting points. A 15 mg LM droplet representing bulk EGaIn shows a peak freezing point of −5.9 °C (onset = −11.2 °C) and a peak melting point of +17.8 °C (onset = 15.7 °C) when subjected to the same heating and cooling cycle. Significantly lowered freezing (from −6 to −84 °C) and melting (from +18 to −26 °C) points of LM phase in the elastomer composite are due to the confinement of LM-droplets to micro-/nanometer length scale and increase in the interfacial and surface forces. For inorganic nanoparticles such as gold and indium, the melting and freezing temperatures are size dependent and decrease as the diameter of the particles is reduced due to the increased effect of surface energy in nanoparticles.[41–43] In pure Ga and Ga-based alloy nanoparticles, co-existence of liquid and solid phases and formation of interfaces between these two phases contribute in suppressing the crystallization temperature and intensify the supercooling effect.[44–47] It should be mentioned that this level of supercooling and melting-point depression in LM-elastomer composites was achieved by tailoring the size and uniformity of LM micro-droplets. For instance, in LMEE specimens with larger micro-droplets (an average diameter of ≈50 µm), a continuous crystallization of LM droplets is observed starting at −60.3 °C and ending with a small additional peak at −82 °C which indicates a lower phase transition rate of LM droplets with smaller diameters (Figure S3, Supporting Information).

2.2. Role of Matrix Materials

LM-droplets were integrated in different polymeric matrices in order to investigate the role of matrix materials on freezing and melting behavior of the liquid inclusions. Microscopic images in **Figure 3**a show the morphology of the LM droplets

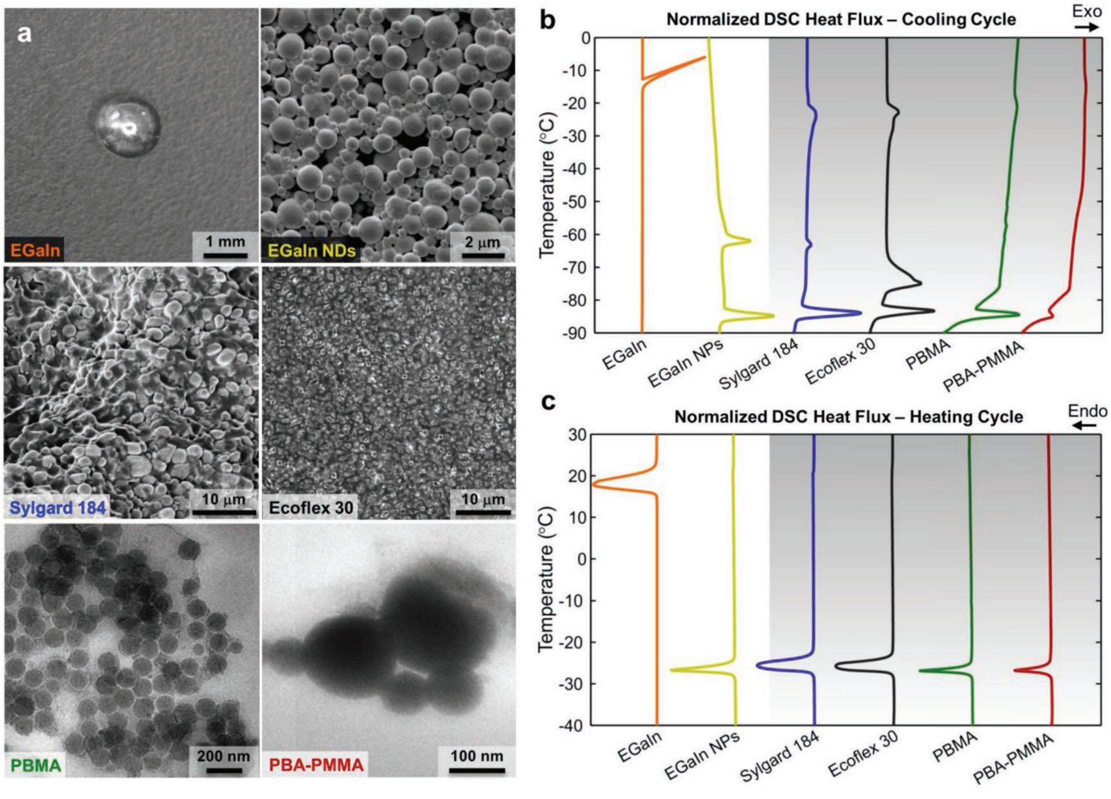

Figure 3. Effect of matrix materials on freezing and melting temperatures of LM-systems. a) Representative images of each sample; a large drop of EGaIn, EGaIn nanoparticles (≈500 nm) without any matrix, EGaIn-Sylgard 184 LMEE, EGaIn-Ecoflex 00–30 LMEE, EGaIn filled PBMA, and EGaIn-PBA-*b*-PMMA composite. b) Exothermic peaks showing the crystallization of bulk EGaIn, EGaIn nanoparticles, and EGaIn composites with different polymer matrices. c) Endothermic peaks indicating the melting temperature of bulk EGaIn, EGaIn nanoparticles, and EGaIn composites with different polymer matrices (shaded background indicates EGaIn composites).

at different size scales with and without polymer matrices. A relatively large droplet of EGaIn (≈15 mg) was used for DSC analysis to reflect the thermal properties of bulk EGaIn as a reference. DSC analysis on EGaIn NDs without any matrix was performed in order to determine whether the presence/absence of the polymer matrix would influence LM supercooling. In addition to the LM-filled PDMS (Sylgard 184), Ecoflex 00–30 was also examined as another representative silicone-based elastomer to fabricate LMEE samples in a similar manner. Furthermore, we considered thermoplastics as a different class of polymer matrices to encapsulate LM droplets and generalize our hypothesis on suppression of crystallization and melting temperature. Through surface-initiated atom transfer radical polymerization (SI-ATRP), EGaIn NDs were stabilized in poly(*n*-butyl acrylate) (PBMA) and poly(*n*-butyl acrylate-*block*-methyl methacrylate) (PBA-*b*-PMMA) as two thermoplastic polymer hybrids.[48]

Figure 3b,c illustrates the normalized DSC heat flux curves of these six compositions and the corresponding phase transition peaks. The largest exothermic peak during the cooling cycle indicates crystallization of EGaIn phase (Figure 3b) and the endothermic peaks during the heating cycle represent the melting point (Figure 3c). Independent of the matrix materials and synthesis process, the freezing and melting temperatures of EGaIn with sufficiently small droplet size appear to be close to −85 and −26 °C, respectively. The same thermal behavior is observed for pure EGaIn NDs (≈500 nm in diameter) without the presence of any polymer, which confirms that the suppression of freezing and melting temperatures is a direct effect of reduced droplet size. This extreme supercooling behavior is in agreement with the previously reported behavior of gallium nanoparticles due to the phase separation and formation of solid core and liquid shell gallium.[44–46] This phenomenon can be explained when the surface energy of nanoparticles is considered in the Gibbs free energy of the system.[49] A recent study showed that EGaIn NDs with an average diameter of ≈180 nm show similar behavior.[47] In this case, a solid indium core with a liquid gallium shell forms during the phase separation at low temperatures (≈−67 °C). Further decrease in temperature results in freezing of the liquid Ga and solidification of the nanoparticle. The free movement of solid indium core and extreme supercooling effect of gallium are plausible explanations for suppressed melting and freezing temperatures of EGaIn nano-/micro droplets. It should be mentioned that the size distribution of EGaIn NDs is polydispersed and the presence of larger LM inclusions can also potentially lead to an additional phase transition peak below −60 °C during the cooling cycle (Figure 3b). Similar peaks are observed for LMEE specimens with Sylgard 184 as the matrix material, which implies the possible co-existence of the solid indium core and liquid gallium shell inside EGaIn droplets. However, this minor phase transition does not show any considerable effect in the stretchability or stiffness of the specimens, as confirmed with the DMA results shown in Figure 2.

LMEE samples with Ecoflex matrix show a relatively large peak between −70 and −80 °C, which corresponds to the freezing of unfilled Ecoflex at this temperature (see Figure S2a, Supporting Information). Similar phase transition temperatures are observed for the encapsulated EGaIn NDs in PBMA (−84.5 and −26.9 °C) and PBA-*b*-PMMA (−85.1 and −26.8 °C) polymers. For these thermoplastic matrices, the surface functionalization of EGaIn droplets resulted in droplet sizes in the range of less than 100–200 nm.[48] No additional phase changes occurred in this case because of the smaller size and more uniform dispersion of the droplets. The thermal stability of SI-ATRP samples further confirms that supercooling of EGaIn droplets is independent of the synthesis method and presence of polymer coating or substrate, and it is not necessarily a result of high mechanical shear mixing which creates an oxide layer on the surface of droplets. Therefore, the suppressed crystallization temperature can be extended to EGaIn nano-/micro droplets synthesized by microfluidic dispensing,[26,50,51] shear mixing,[52] and ultrasonic sonication[8,53,54] with different polymer coatings.[53]

3. LMEE for Wearable Thermoelectric Generators (TEGs)

Stabilizing LM droplets at temperatures below −80 °C significantly broadens the range of potential applications for LM-based electronics and functional structures. For instance, the combination of high thermal conductivity of LMEEs, low Young's modulus, and their stretchability at low temperatures make them suitable for wearable TEGs and heating/cooling devices and wearables. As illustrated in **Figure 4**a, LMEEs can be used as a thermal interface to efficiently transfer body heat to the hot side of the TEG module and also dissipate heat from its cold side. Contrary to flexible TEGs that utilize LM alloy as a soft and stretchable electrical interconnects,[55–57] here the LM elastomer composites are used as a material interface to enhance thermal management in wearable thermoelectric devices. In this hybrid TEG device, the unfilled PDMS in the middle strongly bonds to the LMEE layers and serves as a heat shield between the two sides of the TEG, thereby reducing unwanted heat transfer and energy dissipation. Similar to a conventional heat sink, the LMEE layer on the cold side has a larger surface area for better heat release. Because the TEG unit is embedded in an entirely soft and stretchable package, it can be used as a wearable energy harvester or simply as a heating/cooling wearable device.

First, the influence of the LMEE thermal interface on the Seebeck effect of TEGs is examined to evaluate the practicality of the design. In this test, the devices were subjected to a temperature difference of approximately 37 °C and the open-circuit voltage was measured. As depicted in Figure 4b,c, introducing LMEE as a thermal interface and unfilled PDMS as an insulating layer has minimal effect on the performance of TEG devices when compared to an unpackaged one. Although the presence of LMEE layers means having an additional material interface on each side of the TEG which eliminates the direct contact between TEG and hot/cold surfaces, the soft LMEE interfaces provide a better conformal contact over a large surface area, particular for human body and curved 3D objects. If the TEG is embedded in unfilled PDMS, the generated voltage is significantly lower because of the poor heat transfer of the insulating packaging materials. This result is not limited to a specific size or type of device as similar behavior was

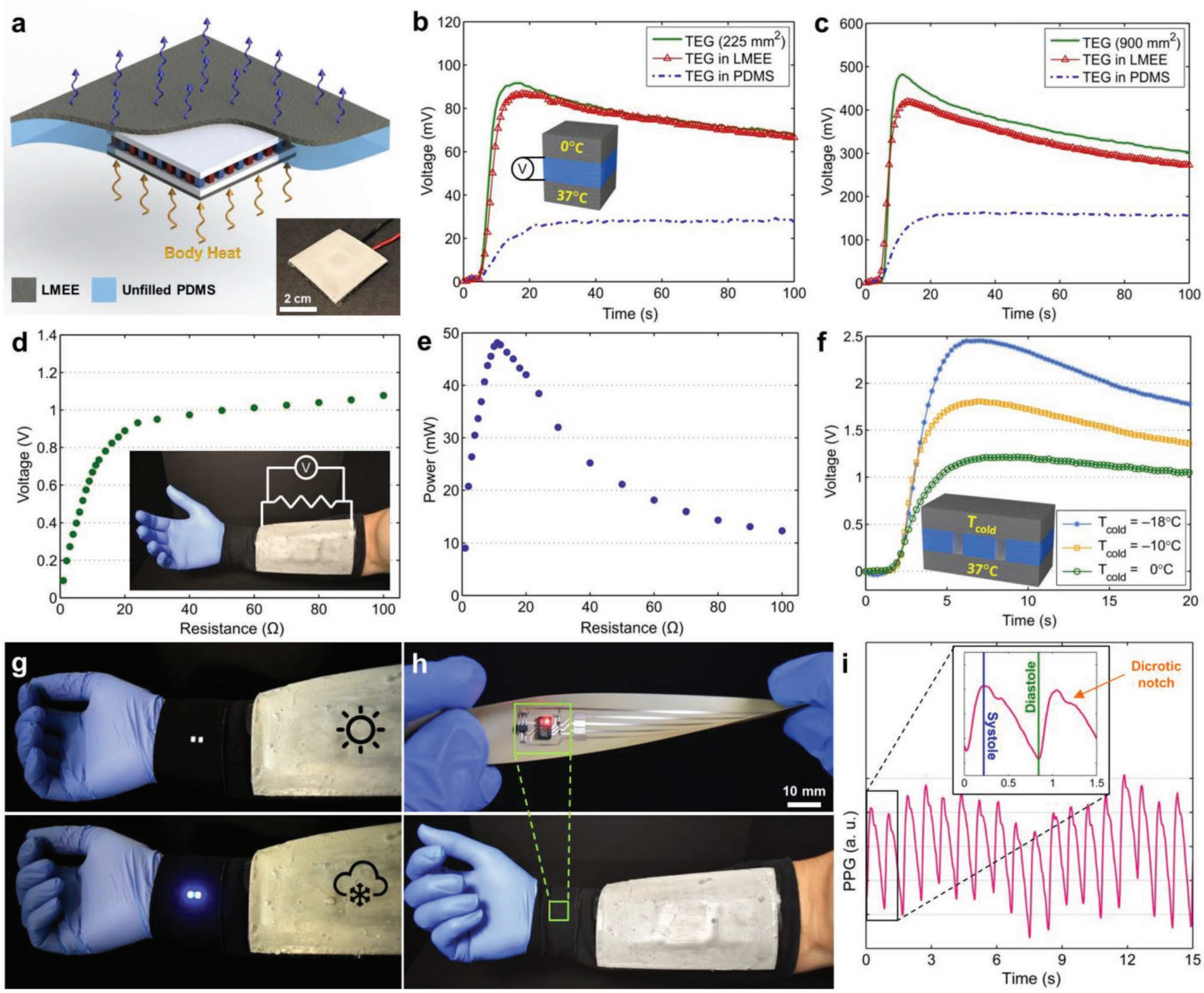

Figure 4. Self-powered wearable electronics for extreme cold environments. a) Schematic of a TEG device with LMEE thermal interface and unfilled PDMS thermal shield. b) Generated open-circuit voltage from 15 mm × 15 mm TEG devices with different packaging (without matrix, LMEE, and unfilled PDMS) when subjected to a 37 °C temperature gradient. c) Generated open-circuit voltage from 30 mm × 30 mm TEG devices with different packaging materials subjected to a 37 °C temperature gradient. d) Measured voltage output from TEG sleeve (inset figure) as a function of load resistance when the cold side (outer LMEE layer) is 0 °C. e) Estimated power from the TEG sleeve under the same temperature gradient. f) Open-circuit voltage from the wearable TEG device when the cold side temperature is set to 0, −10, and −18 °C, which is below the freezing point of bulk EGaIn. g) A self-powered electronic sleeve to power integrated LED lights on a flexible PCB covered. h) An implementation of a wearable pulse oximeter circuit interfaced with a hybrid TEG for heart beat monitoring in extreme cold weathers. i) A representative PPG waveform collected from the self-powered pulse oximetry circuit (inset: detected common features of a cardiac cycle).

obtained for two TEG modules with different dimensions. The 30 mm × 30 mm TEG modules with LMEE interface are able to generate more than 400 mV at first and gradually reach a steady output of 250 mV. This level of voltage generation under only 37 °C temperature difference (approximated to the difference between body temperature and 0 °C surrounding environments) enables application of the TEGs for self-powered wearable electronics. Unlike entirely flexible thermoelectric devices,[58–60] the embedded TEG devices with LMEE interface provide adequate electricity to power small electronics and be used for wireless, wearable bio-monitoring in extreme cold weather conditions.

A self-powered "electronic sleeve" composed of three TEGs was fabricated to demonstrate the application of the tailored LMEE composite as a cold-resistant thermal interface (Figure 4d, inset). The hot side of the TEGs is bonded to a fabric by a thin layer of LMEE and the LMEE-covered cold side is exposed to the atmosphere. This electronic sleeve can be simply interfaced with various circuits printed on flexible materials to make fully functional self-powered wearable electronics at low temperatures. The fabrication process of this wearable thermoelectric sleeve is shown in Figure S4 in the Supporting Information. The power generation capability of the TEG sleeve was estimated by measuring the voltage across different load resistance when the sleeve was subjected to a 37 °C temperature gradient (outer LMEE layer was kept at 0 °C). As shown in Figure 4d, the output voltage increases by increasing the load resistances until it reaches approximately 1.1 V at 100 Ω, which is close to the open-circuit voltage of the device at this temperature gradient. The power generation of the TEG sleeve can be estimated based on the measured voltage and known resistance value.[61,62] As expected, the power is a function of load resistance (Figure 4e) and reaches its maximum value when the internal impedance of device is matched with the load resistor. For the TEG sleeve, the maximum power generation is estimated to approximately 48.1 mW when the optimal load resistor of 11 Ω was used. It should be noted that the generated power with different resistors varying from 1 to 100 Ω remains higher than 10 mW, indicating the high energy harvesting capacity of this soft and flexible TEG device. The temperature on the cold side was set to 0 °C as a threshold to determine the lowest required temperature gradient to have a thermoelectric sleeve that functions in cold conditions. As shown in Figure 4f, reducing the temperature on the cold side (outer LMEE layer) of the sleeve to lower temperatures significantly increases the output voltage, up to 2.45 V at −18 °C, at temperature at which bulk EGaIn will freeze.

The high energy harvesting capability of the LMEE-based thermoelectric sleeve can enable interfacing with different wearable circuits and eliminates the need for battery cells. For instance, when the temperature of the cold side is reduced to 0 °C, the generated power from TEG sleeve is sufficient to light up two blue light-emitting diodes (LEDs; Figure 4g). Most significantly, this electronic sleeve is able to power bioelectric circuits under the same temperature conditions. As shown in Figure 4h, the harvested thermal energy is utilized to power a pulse oximetry circuit for noninvasive measurement of the blood oxygen saturation (SpO_2) and heart rate. Similar to other miniaturized wearable pulse oximetry systems, the captured and filtered photoplethysmogram (PPG) forms can be used for personal health monitoring.[63–67] The circuit was fabricated on a flexible printed circuit board (PCB) and attached to a fabric wrist band in order to achieve good conformal contact with the wrist. Additional details on the fabrication process and electronic circuit are presented in the Supporting Information and Figure S5 (Supporting Information). The use of fabric also preserved the device's lightweight properties and made it comfortable to wear. Figure 4i shows a PPG waveform collected from the wearable pulse oximetry unit that was powered from energy harvested from a 37 °C thermal gradient. The heart muscle contraction (systole), relaxation (diastole), and secondary upstroke (dicrotic notch) can be observed in the collected PPG signal (Figure 4i, inset). This result shows the feasibility of using wearable TEGs to power wearable biosensing electronics for real-time heart rate monitoring in extreme cold conditions (< 0 °C). It should be mentioned that the same electronic sleeve can be utilized as a heating or cooling garment when electrical power is supplied to the embedded thermoelectric.

4. Conclusion

In this study, we report a class of LM polymer composites that remain mechanically compliant and fully functional in extremely low temperatures, < −80 °C. This temperature is significantly lower than the minimum working temperature of common fluidic LM systems. The extended temperature range was achieved by controlling the LM droplet size (to less than 3 µm in diameter) and through appropriate selection of the polymer matrix. Because the droplets stay in the liquid phase and the surrounding polymer remains soft, conformal, and stretchable, the composite is able to maintain its mechanical compliance at these reduced temperatures. Our studies also suggest that the suppressed freezing and melting temperatures of LM droplets are independent of polymer matrix and synthesis process. We demonstrated this phenomenon by examining various types of thermoset and thermoplastic polymers and utilize both mechanical shear mixing and surface functionalization processes to encapsulate LM droplets at the scale of nano-/micrometer. These findings provide new insights on the crystallization of Ga-based alloys and broaden the feasible applications of this class of soft multifunctional materials. We show the practicality of these composites in wearable thermoelectrics by fabricating self-powered bio-electronic sleeve that monitors an individual's heart rate in cold weather conditions. Such a device benefits from the combination of high thermal conductivity and mechanical compliance at low temperatures that is made possible with the LMEE composites presented here.

5. Experimental Section

Synthesis of LM Polymer Composites: EGaIn (75 wt% Ga and 25 wt% In) was prepared by mixing raw Ga and In (Rotometals Inc.) at 195 °C and continuous stirring for 12 h. An immersion shear mixer (OS20-S LED Digital Overhead Stirrer, Scilogex LLC.) at a speed of 2200 rpm for 30 min was utilized to disperse LM droplets in silicone-based elastomer matrices. PDMS (Sylgard 184, Dow Corning Corp.) and Ecoflex 00–30 (Smooth-On Inc.) were used as matrix materials to fabricate LMEE composites with 50% volume fraction of EGaIn. The mass of each mixing batch was in the range of 200–400 g which showed the scalability of this fabrication process. For Sylgard 184, the LM was added to the base part during immersion mixing and then the curing agent was added with a 10:1 ratio and mixed for 1 min in a planetary centrifugal mixer (AR-100 THINKY Crop.) prior to the casting step. For Ecoflex 00–30, an equal amount of LM was added to part A and B and then mixed in smaller batches prior to the use in the planetary centrifugal shear mixer. After mixing, the cast samples were naturally degassed at atmospheric pressure and room temperature for 2 h then cured in an oven at 100 °C for 1 h. SI-ATRP was utilized as an alternative synthesis process to prepare LM composites with EGaIn NDs. The full details of SI-ATRP synthesis for EGaIn-PBMA and EGaIn-PBA-b-PMMA composites can be found elsewhere.[48] EGaIn NDs were synthesized by ultrasonication of bulk EGaIn in ethanol without using any surfactant.[8] Formation of an oxide skin on the NDs stabilized them in the solution. The solvent was evaporated in a vacuum oven prior to thermal characterization.

DSC: DSC measurements were performed on a TA Instruments Q20. Micro-/nano LM composite solutions were directly drop cast into Tzero aluminum pans and cured in the oven to provide a full contact between specimen and inner surface of the pans. Prior to the experiment, the removal of solvent was performed at room temperature and followed by heating the pan to 100 °C. For heating and cooling DSC runs, 5–15 mg specimens were cooled to −90 °C and then heated to 35 °C at a rate of 5 °C min^{-1} under a constant flow of nitrogen with a rate of 50 mL min^{-1}.

DMA: RSA-G2 Solids Analyzer (TA Instruments) was utilized to examine the viscoelastic properties and phase transition of LMEE specimens. The "Tension Film Fiber" was used as the clamping system for axial loading of the samples (10 mm × 8 mm × 1 mm) under controlled strain of 1% and a frequency of 1 Hz. Under a rate of 5 °C min^{-1}, the specimens were cooled down to −90 °C and heated to 35 °C using liquid nitrogen.

Microscopy Imaging: Scanning electron microscopy (SEM) was performed on a Quanta 600 operating at 5 kV and transmission electron microscopy (TEM) was conducted on samples using a JEOL 2000EX operating at 200 kV. The 3D nanoscale X-ray computational tomography (3D Nano-CT) of LMEE composite was captured and analyzed by UltraXRM L200 (Xradia, Inc.).

Self-Powered Wearable Electronics: LMEE was utilized as a flexible thermal adhesive to mount TEGs on cotton spandex fabric and also a thermal interface to release the heat. This add-on rubbery power harvester on fabric sleeve was interfaced with bioelectric circuits printed on Pyralux copper-clad laminates (FR8515R, Dupont). The details of fabrication process and circuit design can be found in the Supporting Information.

Supporting Information

Supporting Information is available from the Wiley Online Library or from the author.

Acknowledgements

This research was supported by Air Force Office of Scientific Research (AFOSR) Multidisciplinary University Research Initiative (FA9550-18-1-0566; Program Manager: K. Goretta) and the National Science Foundation Division of Civil, Mechanical, and Manufacturing Innovation (CMMI; Dr. Mary M. Toney; Award 1635824). The authors thank Leiming Hu for the Nano-CT scan, Zhao Lu for TEM imaging, and Kadri Bugra Ozutemiz for helpful guidance on the design of the pulse oximeter circuit.

Conflict of Interest

The authors declare no conflict of interest.

Keywords

extreme conditions, liquid metals, soft multifunctional composites, thermal stability, thermoelectric generators, wearable electronics

Received: July 26, 2019
Revised: August 11, 2019
Published online:

[1] N. Kazem, T. Hellebrekers, C. Majidi, *Adv. Mater.* **2017**, *29*, 1605985.
[2] Y. Lin, C. Cooper, M. Wang, J. J. Adams, J. Genzer, M. D. Dickey, *Small* **2015**, *11*, 6397.
[3] H. Wang, Y. Yao, Z. He, W. Rao, L. Hu, S. Chen, J. Lin, J. Gao, P. Zhang, X. Sun, *Adv. Mater.* **2019**, *31*, 1901337.
[4] J. Wang, M. Lin, S. Park, P. S. Lee, *Mater. Today* **2018**, *21*, 508.
[5] S. H. Jeong, S. Zhang, K. Hjort, J. Hilborn, Z. Wu, *Adv. Mater.* **2016**, *28*, 5830.
[6] A. Koh, J. Sietins, G. Slipher, R. Mrozek, *J. Mater. Res.* **2018**, *33*, 2443.
[7] M. D. Bartlett, A. Fassler, N. Kazem, E. J. Markvicka, P. Mandal, C. Majidi, *Adv. Mater.* **2016**, *28*, 3726.
[8] C. Pan, E. J. Markvicka, M. H. Malakooti, J. Yan, L. Hu, K. Matyjaszewski, C. Majidi, *Adv. Mater.* **2019**, *31*, 1900663.
[9] R. Tutika, S. Kmiec, A. T. Haque, S. W. Martin, M. D. Bartlett, *ACS Appl. Mater. Interfaces* **2019**, *11*, 17873.
[10] M. D. Bartlett, N. Kazem, M. J. Powell-Palm, X. Huang, W. Sun, J. A. Malen, C. Majidi, *Proc. Natl. Acad. Sci. U. S. A.* **2017**, *114*, 2143.
[11] S. H. Jeong, S. Chen, J. Huo, E. K. Gamstedt, J. Liu, S. Zhang, Z. Zhang, K. Hjort, Z. Wu, *Sci. Rep.* **2015**, *5*, 18257.
[12] R. Tutika, S. H. Zhou, R. E. Napolitano, M. D. Bartlett, *Adv. Funct. Mater.* **2018**, *28*, 1804336.
[13] P. Fan, Z. Sun, Y. Wang, H. Chang, P. Zhang, S. Yao, C. Lu, W. Rao, J. Liu, *RSC Adv.* **2018**, *8*, 16232.
[14] A. Fassler, C. Majidi, *Adv. Mater.* **2015**, *27*, 1928.
[15] X. Li, M. Li, L. Zong, X. Wu, J. You, P. Du, C. Li, *Adv. Funct. Mater.* **2018**, *28*, 1804197.
[16] S. Liang, Y. Li, Y. Chen, J. Yang, T. Zhu, D. Zhu, C. He, Y. Liu, S. Handschuh-Wang, X. Zhou, *J. Mater. Chem. C* **2017**, *5*, 1586.
[17] J. Wang, G. Cai, S. Li, D. Gao, J. Xiong, P. S. Lee, *Adv. Mater.* **2018**, *30*, 1706157.
[18] B. Deng, G. J. Cheng, *Adv. Mater.* **2019**, *31*, 1807811.
[19] N. Kazem, M. D. Bartlett, C. Majidi, *Adv. Mater.* **2018**, *30*, 1706594.
[20] P. S. Owuor, S. Hiremath, A. C. Chipara, R. Vajtai, J. Lou, D. R. Mahapatra, C. S. Tiwary, P. M. Ajayan, *Adv. Mater. Interfaces* **2017**, *4*, 1700240.
[21] H. Peng, Y. Xin, J. Xu, H. Liu, J. Zhang, *Mater. Horiz.* **2019**, *6*, 618.
[22] C. B. Cooper, I. D. Joshipura, D. P. Parekh, J. Norkett, R. Mailen, V. M. Miller, J. Genzer, M. D. Dickey, *Sci. Adv.* **2019**, *5*, eaat4600.
[23] E. J. Markvicka, M. D. Bartlett, X. Huang, C. Majidi, *Nat. Mater.* **2018**, *17*, 618.
[24] Y. Xin, H. Peng, J. Xu, J. Zhang, *Adv. Funct. Mater.* **2019**, *29*, 1808989.
[25] X. Guo, Y. Ding, L. Xue, L. Zhang, C. Zhang, J. B. Goodenough, G. Yu, *Adv. Funct. Mater.* **2018**, *28*, 1804649.
[26] M. D. Dickey, R. C. Chiechi, R. J. Larsen, E. A. Weiss, D. A. Weitz, G. M. Whitesides, *Adv. Funct. Mater.* **2008**, *18*, 1097.
[27] A. C. Siegel, D. A. Bruzewicz, D. B. Weibel, G. M. Whitesides, *Adv. Mater.* **2007**, *19*, 727.
[28] T. Daeneke, K. Khoshmanesh, N. Mahmood, I. De Castro, D. Esrafilzadeh, S. Barrow, M. Dickey, K. Kalantar-Zadeh, *Chem. Soc. Rev.* **2018**, *47*, 4073.
[29] L. Teng, S. Ye, S. Handschuh-Wang, X. Zhou, T. Gan, X. Zhou, *Adv. Funct. Mater.* **2019**, *29*, 1808739.
[30] S. Cheng, Z. Wu, *Lab Chip* **2012**, *12*, 2782.
[31] S. Yu, M. Kaviany, *J. Chem. Phys.* **2014**, *140*, 064303.
[32] Q. Xu, N. Oudalov, Q. Guo, H. M. Jaeger, E. Brown, *Phys. Fluids* **2012**, *24*, 063101.
[33] R. K. Kramer, J. W. Boley, H. A. Stone, J. C. Weaver, R. J. Wood, *Langmuir* **2014**, *30*, 533.
[34] J. Kim, S. Kim, J. So, K. Kim, H. Koo, *ACS Appl. Mater. Interfaces* **2018**, *10*, 17448.
[35] L. Bosio, C. Windsor, *Phys. Rev. Lett.* **1975**, *35*, 1652.
[36] S. Risse, B. Kussmaul, H. Krüger, G. Kofod, *RSC Adv.* **2012**, *2*, 9029.
[37] F. B. Madsen, A. E. Daugaard, S. Hvilsted, A. L. Skov, *Macromol. Rapid Commun.* **2016**, *37*, 378.
[38] L. Tang, H. Zhang, S. Sprenger, L. Ye, Z. Zhang, *Compos. Sci. Technol.* **2012**, *72*, 558.
[39] D. McCoul, W. Hu, M. Gao, V. Mehta, Q. Pei, *Adv. Electron. Mater.* **2016**, *2*, 1500407.
[40] N. Kazem, *Ph.D. Thesis*, Carnegie Mellon University, Pittsburgh, PA **2018**.
[41] P. Buffat, J. P. Borel, *Phys. Rev. A* **1976**, *13*, 2287.
[42] K. Unruh, T. Huber, C. Huber, *Phys. Rev. B* **1993**, *48*, 9021.
[43] R. R. Vanfleet, J. Mochel, *Surf. Sci.* **1995**, *341*, 40.
[44] G. Parravicini, A. Stella, P. Ghigna, G. Spinolo, A. Migliori, F. d'Acapito, R. Kofman, *Appl. Phys. Lett.* **2006**, *89*, 033123.

[45] A. Yamaguchi, Y. Mashima, T. Iyoda, *Angew. Chem., Int. Ed.* **2015**, *54*, 12809.
[46] M. Losurdo, A. Suvorova, S. Rubanov, K. Hingerl, A. S. Brown, *Nat. Mater.* **2016**, *15*, 995.
[47] S. Tang, D. R. Mitchell, Q. Zhao, D. Yuan, G. Yun, Y. Zhang, R. Qiao, Y. Lin, M. D. Dickey, W. Li, *Matter* **2019**, *1*, 192.
[48] J. Yan, M. H. Malakooti, Z. Lu, Z. Wang, N. Kazem, C. Pan, M. R. Bockstaller, C. Majidi, K. Matyjaszewski, *Nat. Nanotechnol.* **2019**, *14*, 684.
[49] A. Shirinyan, M. Wautelet, *Nanotechnology* **2004**, *15*, 1720.
[50] T. Hutter, W. C. Bauer, S. R. Elliott, W. T. Huck, *Adv. Funct. Mater.* **2012**, *22*, 2624.
[51] S. Tang, R. Qiao, S. Yan, D. Yuan, Q. Zhao, G. Yun, T. P. Davis, W. Li, *Small* **2018**, *14*, 1800118.
[52] I. D. Tevis, L. B. Newcomb, M. Thuo, *Langmuir* **2014**, *30*, 14308.
[53] T. Gan, W. Shang, S. Handschuh-Wang, X. Zhou, *Small* **2019**, *15*, 1804838.
[54] L. R. Finkenauer, Q. Lu, I. F. Hakem, C. Majidi, M. R. Bockstaller, *Langmuir* **2017**, *33*, 9703.
[55] F. Suarez, D. P. Parekh, C. Ladd, D. Vashaee, M. D. Dickey, M. C. Öztürk, *Appl. Energy* **2017**, *202*, 736.
[56] S. H. Jeong, F. J. Cruz, S. Chen, L. Gravier, J. Liu, Z. Wu, K. Hjort, S. Zhang, Z. Zhang, *ACS Appl. Mater. Interfaces* **2017**, *9*, 15791.
[57] B. Chen, M. Kruse, B. Xu, R. Tutika, W. Zheng, M. D. Bartlett, Y. Wu, J. C. Claussen, *Nanoscale* **2019**, *11*, 5222.
[58] S. J. Kim, J. H. We, B. J. Cho, *Energy Environ. Sci.* **2014**, *7*, 1959.
[59] J. Bahk, H. Fang, K. Yazawa, A. Shakouri, *J. Mater. Chem. C* **2015**, *3*, 10362.
[60] H. Wu, Y. Huang, F. Xu, Y. Duan, Z. Yin, *Adv. Mater.* **2016**, *28*, 9881.
[61] M. H. Malakooti, B. A. Patterson, H. Hwang, H. A. Sodano, *Energy Environ. Sci.* **2016**, *9*, 634.
[62] S. Hong, Y. Gu, J. K. Seo, J. Wang, P. Liu, Y. S. Meng, S. Xu, R. Chen, *Sci. Adv.* **2019**, *5*, eaaw0536.
[63] C. M. Lochner, Y. Khan, A. Pierre, A. C. Arias, *Nat. Commun.* **2014**, *5*, 5745.
[64] T. Lu, E. J. Markvicka, Y. Jin, C. Majidi, *ACS Appl. Mater. Interfaces* **2017**, *9*, 22055.
[65] J. Kim, P. Gutruf, A. M. Chiarelli, S. Y. Heo, K. Cho, Z. Xie, A. Banks, S. Han, K. Jang, J. W. Lee, *Adv. Funct. Mater.* **2017**, *27*, 1604373.
[66] Y. H. Lee, O. Y. Kweon, H. Kim, J. H. Yoo, S. G. Han, J. H. Oh, *J. Mater. Chem. C* **2018**, *6*, 8569.
[67] J. Heikenfeld, A. Jajack, J. Rogers, P. Gutruf, L. Tian, T. Pan, R. Li, M. Khine, J. Kim, J. Wang, *Lab Chip* **2018**, *18*, 217.